DALTON
FULL PAPER

Spectroscopic and electron paramagnetic resonance behavior of trinuclear metallic clusters encapsulated in $[M^{n+}{}_3(H_2O)_x(BiW_9O_{33})_2]^{(18-3n)-}$ heteropolyanion (M^{n+} = $(VO)^{II}$, x = 0 and M^{n+} = Cr^{III}, Mn^{II}, Fe^{III}, Co^{II}, Ni^{II}, Cu^{II}, x = 3)†

Dan Rusu,[a] Cora Crăciun,[b] Anne-Laure Barra,[c] Leontin David,*[b] Mariana Rusu,[d] Cristina Roşu,[d] Onuc Cozar[b] and Gheorghe Marcu[d]

[a] *Department of Chemical-Physics, Medical and Pharmaceutical University, 3400, Cluj-Napoca, Romania*
[b] *Department of Physics, "Babeş-Bolyai" University, 3400, Cluj-Napoca, Romania*
[c] *High Magnetic Field Laboratory, MPI-CNRS, 38042 Grenoble, France*
[d] *Department of Chemistry, "Babeş-Bolyai" University, 3400, Cluj-Napoca, Romania*

Received 4th June 2001, Accepted 2nd August 2001
First published as an Advance Article on the web 17th September 2001

A new series of sodium/potassium salts of sandwich-type $[M^{n+}{}_3(H_2O)_x(BiW_9O_{33})_2]^{(18-3n)-}$ heteropolyanions (M^{n+} = $(VO)^{II}$, x = 0 (**1**) and M^{n+} = Cr^{III} (**2**), Mn^{II} (**3**), Fe^{III} (**4**), Co^{II} (**5**), Ni^{II} (**6**), Cu^{II} (**7**), x = 3) were synthesized and characterized by means of elemental analyses, thermogravimetry, FT-IR, UV-VIS, EPR and HF-EPR spectroscopy. FT-IR data are proof of the heteropolyanion frame formation and indicate the co-ordination of each transition metal at two corner-shared octahedra from the trivacant Keggin fragments. The low shift of the $\nu_{asym}(Bi–O_a)$ band in the spectra of the Cu^{II} and Fe^{III} compounds relative to the ligand spectrum suggests a sterically-inert s^2 lone pair on each Bi^{III} ion. The charge transfer band $p_\pi(O_t)\longrightarrow d_{\pi^*}(W)$ at 193.6 nm is not affected by the co-ordination of the metals, but the $p_\pi(O_{c,e})\longrightarrow d_{\pi^*}(W)$ band shifts towards higher energies for Cr^{III} and Fe^{III} complexes or lower energies for the other complexes. d–d transitions obtained in the VIS spectra of the complexes have been interpreted in terms of five-co-ordination of every transition metal and a distorted square-pyramidal local symmetry. EPR and HF-EPR data show the presence of small antiferromagnetic interactions in the spin frustrated trinuclear metallic clusters ($J = -4.116$ cm^{-1} for the Cr^{III} complex, $J = -2.074$ cm^{-1} for the Mn^{II} complex). Two species with different degrees of rhombical distortion have been identified in the case of the Fe^{III} (D_1 = 1.5 cm^{-1}, E_1 = 0.12 cm^{-1} and D_2 = 1.5 cm^{-1}, E_2 = 0.5 cm^{-1}) and Co^{II} (g_{x1} = 5.021, g_{y1} = 3.561, g_{z1} = 2.401 and g_{x2} = 5.776, g_{y2} = 3.813, g_{z2} = 2.850) samples.

Introduction

During the last years, sandwich-type heteropolyoxometalates (HPOM) encapsulating clusters of early transition metals have received much attention both from applied (in material science,[1–3] medicine,[4,5] catalysis[6–8]) and fundamental research perspectives.[9–11] The great advantage of these complexes is the possibility of varying either the type of the metallic cluster (its structural topology and the nature of the transition metals) or the heteroatom.[12,13] The proximity of the transition metals possessing unpaired electrons facilitates their coupling through exchange, superexchange or dipolar interactions. These are the starting points for magnetic cluster formation.[14] The metallic cluster is usually encapsulated between two Keggin or Dawson–Wells trivacant fragments.

Heteroatoms P^V, As^V, Si^{IV} and Ge^{IV} are tetrahedrally co-ordinated by oxygen atoms in these fragments and the fourth oxygen acting toward the lacunary region is involved in co-ordination to the metallic cluster. On the other hand, the heteroatoms As^{III}, Sb^{III} and Bi^{III} are surrounded pyramidally by three oxygen atoms.[15] They display interesting structures due to the stereochemical effect of the lone pair orbital electrons located on top of the trigonal pyramid.[16]

In contrast with the As^{III} and Sb^{III} containing heteropolyoxometalates which have been intensively studied,[17–21] only a little work has been carried out on the Bi^{III} analogues. Several HPOM as the bis-undecatungstobismutate complex $[Bi_2W_{22}O_{74}(OH)_2]^{12-}$, its 3d transition-metal-disubstituted complexes $[Bi_2W_{20}M_2O_{70}(H_2O)_6]^{(14-2n)-}$ (M = Mn^{II}, Fe^{III}, Co^{II} and Zn^{II}) and the $Na_8(NH_4)_{2.5}[Sn_{1.5}\{WO_2(OH)\}_{0.5}(WO_2)_2(BiW_9O_{33})_2]\cdot 36.5H_2O$ heteropolyoxometalate composed of trivacant β-B-(BiW_9O_{33}) units,[16,22–25] the polyanion[26] $[H_3BiW_{18}O_{60}]^{6-}$ and the salt[27] $K_{11}H[(BiW_9O_{33})_3Bi_6(OH)_3(H_2O)_3V_4O_{10}]\cdot 25H_2O$ containing α-B-(BiW_9O_{33}) units have been reported.

In this context, our research focuses on the investigation of Bi^{III} based sandwich-type heteropolyoxometalates incorporating three 3d transition metals. In similar compounds but having As^{III} or Sb^{III} as heteroatoms, each transition metal is five-co-ordinated by oxygen atoms,[10,28] except in the case of the Cu^{II} compound,[29] which can present mixed four- and five-co-ordination environments. Four of the oxygen atoms belong to the Keggin fragments (two atoms to each unit) and the fifth oxygen belongs to an apical water molecule[30] or to a vanadyl group in complexes with V^{IV}. The three transition metals are arranged in an isosceles or equilateral triangle at distances of about 4.2–5.1 Å which prevent the direct overlapping of their 3d orbitals.[10,29] The superexchange (if present) is realized by involving the heteropolyoxometalate frame.[31]

In this paper we report the synthesis and physical properties of the new series of sodium/potassium salts of the sandwich-type $[M^{n+}{}_3(H_2O)_x(BiW_9O_{33})_2]^{(18-3n)-}$ (M^{n+} = $(VO)^{II}$, x = 0 (**1**) and M^{n+} = Cr^{III} (**2**), Mn^{II} (**3**), Fe^{III} (**4**), Co^{II} (**5**), Ni^{II} (**6**), Cu^{II} (**7**), x = 3) heteropolyanions (Fig. 1). In order to obtain information about the co-ordination of the metallic ions to the trivacant

† Electronic supplementary information (ESI) available: IR data; X-band EPR spectra of the complexes **2**, **3**, **5**, **7**; estimation of the exchange constant from the linewidth of the HF-EPR spectra of the complex **3**. See http://www.rsc.org/suppdata/dt/b1/b104848c/

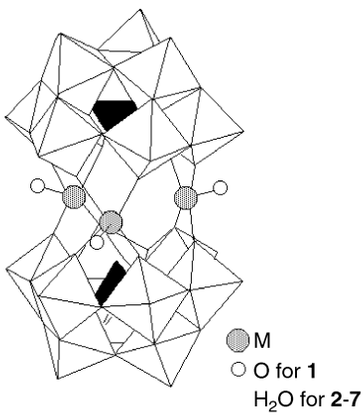

Fig. 1 The structure of the $[M^{n+}{}_3(H_2O)_x(BiW_9O_{33})_2]^{(18-3n)-}$ heteropolyanion. (The empty polyhedra are WO_6 units and the full trigonal pyramids are BiO_3.)

ligand, their oxidation state and the local symmetry around them, the FT-IR and UV-VIS measurements were performed. Precious information on the spin state of the metallic cluster and the type of metal–metal coupling were provided by the EPR and HF-EPR spectra in the 5–293 K temperature range.

Results and discussion

Infrared data

The bending vibrational bands of the heteropolyoxometalate frame appearing in the 300–500 cm^{-1} range obscure the metal–oxygen bond vibrations.[32] Therefore, the analysis of the co-ordination mode of the transition metal ions was made by means of comparison between the FT-IR spectra of the sandwich-type complexes with those of the $Na_9[BiW_9O_{33}]\cdot 14H_2O$ ligand (see ESI) (Fig. 2). The relatively small shift of the $\nu_{asym}(W{=}O_t)$ vibration band, either towards lower frequencies (by 11 cm^{-1} for **3**, 4 cm^{-1} for **5**, 4 cm^{-1} for **2** and 3 cm^{-1} for **4**) or towards higher frequencies for complexes with metals providing a smaller number of unpaired electrons (by 1 cm^{-1} for **7**, 3 cm^{-1} for **6** and 4 cm^{-1} for **1**) is due to the fact that the terminal O_d atoms are not involved in the co-ordination. The decrease in the metallic complexes of the $\nu_{asym}(W{-}O_e{-}W)$ frequencies for the tricentric bonds of edge-sharing WO_6 octahedra indicates the lengthening of these bonds after the metallic ion complexation.[33] Two vibration bands for tricentric $W{-}O_c{-}W$ bonds of the corner-sharing WO_6 octahedra appear in the FT-IR spectra of the complexes (except those with Cu^{II} and Cr^{III} ions), suggesting that two nonequivalent bondings of this type are present.[34] One of them belongs to the belt region (with six octahedra) of the trivacant Keggin units and has a higher vibrational frequency than in the ligand and the other belongs to the cap region (with three octahedra) and presents a lower frequency. The opposite shift of $\nu_{asym}(W{-}O_e{-}W)$ and $\nu_{asym}(W{-}O_c{-}W)$ frequencies for the bondings from the belt region shows the co-ordination of each metallic ion at oxygen atoms from corner-sharing octahedra.[35]

The $\nu_{asym}(Bi{-}O_a)$ frequency appearing in the ligand spectrum at 843 cm^{-1} is red shifted by 11 cm^{-1} in the spectrum of complex **7** and blue shifted by 5 cm^{-1} for complex **4** because of the sterically-inert s^2 lone pair on each Bi^{III} ion.[29]

The shoulders on the very broad $\nu_{asym}(OH)$ vibration band (3000–3600 cm^{-1} region) are due to the coexistence of the crystallization and coordinated water molecules.[36]

Electronic spectroscopy

The UV electronic spectra of the sandwich-type complexes and of the ligand (Fig. 3) contain two bands characteristic for the ligand to metal charge transfer in the heteropolyoxometalate frame. The more intense band corresponding to the $p_\pi(O_t)\longrightarrow d_{\pi^*}(W)$ transitions[37] is centered at 51653 cm^{-1} (193.6 nm) both in the ligand and complexes spectra. This is in agreement with the co-ordination of the metallic ions in the lacunary region of the trivacant ligand and not to the terminal oxygen atoms. The broader band centered at 39355 cm^{-1} (254.1 nm) in the ligand spectrum belongs to the $p_\pi(O_{c,e})\longrightarrow d_{\pi^*}(W)$ charge transfer transition in the tricentric bonds.[38] This band is shifted towards higher energies in the case of complexes **2** (at 38986 cm^{-1}/256.5 nm) and **4** (38835 cm^{-1}/257.5 nm) when it is nearly masked by the first band, but towards lower energies for the other more stable complexes (**1**: 39604 cm^{-1}/252.5 nm, **3**: 39526 cm^{-1}/253.0 nm, **5**: 39432 cm^{-1}/253.6 nm, **6**: 39479 cm^{-1}/253.3 nm, **7**: 39888 cm^{-1}/250.7 nm).

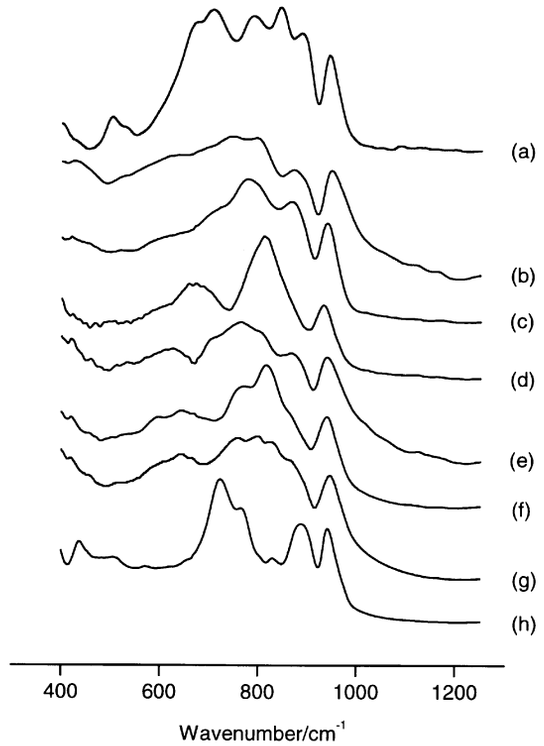

Fig. 2 FT-IR spectra of the ligand (a) and sandwich-type complexes: (b) **1**, (c) **2**, (d) **3**, (e) **4**, (f) **5**, (g) **6**, (h) **7**.

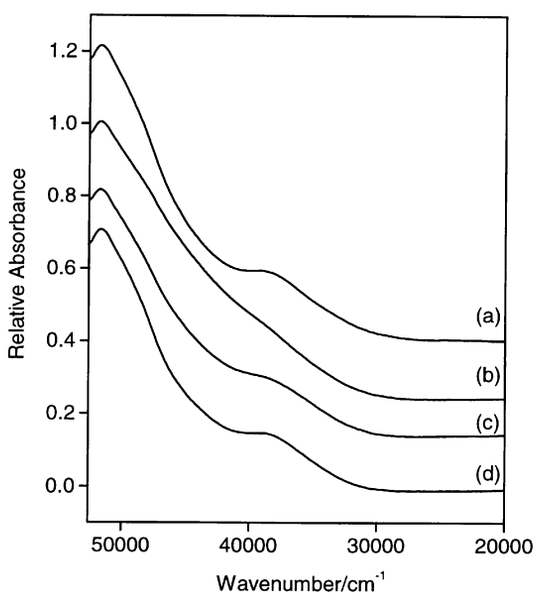

Fig. 3 UV spectra of the ligand (a) and metallic complexes: (a) **2**, (c) **6**, (d) **3**, obtained in 5×10^{-5} mol l^{-1} aqueous solution.

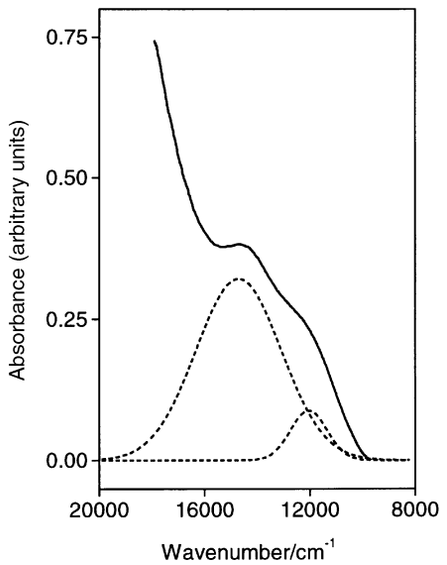

Fig. 4 The visible electronic spectrum of complex **1** in 5×10^{-3} mol l^{-1} aqueous solution. The Gaussian components are represented with dashed lines.

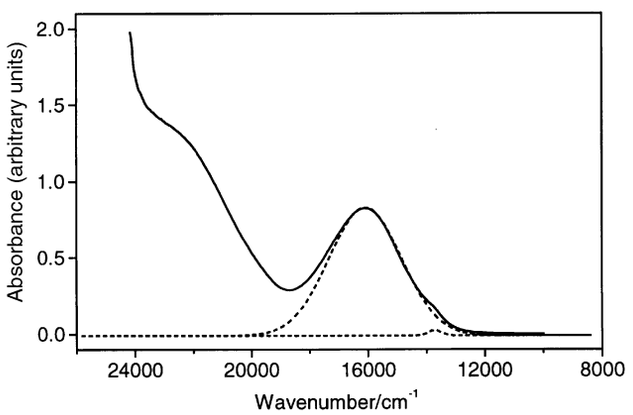

Fig. 5 The visible electronic spectrum of complex **2** in 5×10^{-3} mol l^{-1} aqueous solution. The Gaussian components are represented with dashed lines.

Information about the local environment of 3d metal ions in complexes **1**–**7** have been obtained by means of d–d transitions from the visible electronic spectra performed in aqueous solutions.

The VIS spectrum of complex **1** (Fig. 4) shows a band with a shoulder at ≈15000 cm^{-1} and a very strong absorption at higher wavenumbers. This strong absorption is due to the $V^{IV} \longrightarrow W^{VI}$ charge transfer transition, realized through the oxygen atoms.[39] Two absorptions, centered at 12040 cm^{-1} and 14705 cm^{-1} were obtained by Gaussian deconvolution of the broad feature at ≈15000 cm^{-1}. These are related to the $^2B_2(d_{xy}) \longrightarrow {}^2E(d_{xz,yz})$ (I) and $^2B_2(d_{xy}) \longrightarrow {}^2B_1(d_{x^2-y^2})$ (II) transition bands in Ballhausen and Gray molecular orbital theory for a vanadyl ion in C_{4v} local symmetry.[40]

The electronic spectrum of complex **2** (Fig. 5) presents a very broad band centered at ≈16090 cm^{-1} and a shoulder at ≈13715 cm^{-1}. Such d–d bands were previously reported for five-co-ordinated Cr^{III} ions and are assignable to $^4A_2 \longrightarrow {}^4B_2(^4T_2)$ and $^4A_2 \longrightarrow {}^4E(^4T_2)$ transitions.[41] The spectrum also shows a shoulder at ≈22500 cm^{-1} for the $^4A_2 \longrightarrow {}^4E(^4T_1)$ transition, which is superposed on the charge transfer band.

The very intense charge transfer band of complex **3** situated at wavenumbers higher than 16000 cm^{-1} hides d–d transitions of the Mn^{II} ions. There is a shoulder at ≈17940 cm^{-1} which could be attributed to the transition from the $^6A_1$ ground state

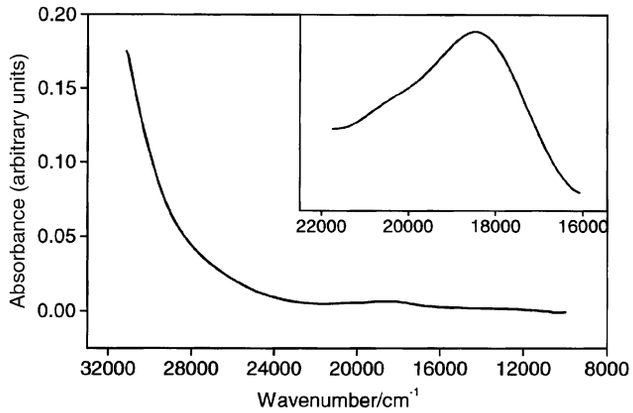

Fig. 6 The visible electronic spectrum of complex **5** in 5×10^{-3} mol l^{-1} aqueous solution. The spectrum obtained in 5×10^{-2} mol l^{-1} aqueous solution is presented in the inset.

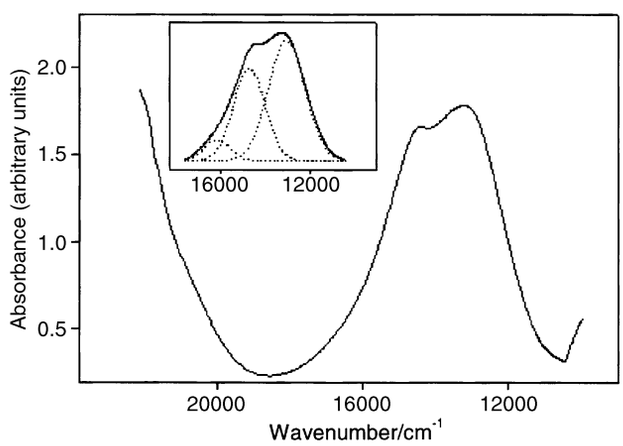

Fig. 7 The visible electronic spectrum of complex **6** in 5×10^{-3} mol l^{-1} aqueous solution. The Gaussian components are represented with dashed lines in the inset.

to one of the components of the $^4T_1(G)$ excited state, in a penta-co-ordinate Mn^{II} system.[42a] However, the lack of other bands in the spectrum makes any conclusion from the VIS spectrum concerning the environment of Mn^{II} to be ambiguous. The same situation is encountered in the VIS spectrum of complex **4**, which contains an $Fe^{III} \longleftarrow O$ charge transfer band starting at about 20000 cm^{-1} and a shoulder at ≈21000 cm^{-1}.[43]

Complex **5** has very weak absorptions in the 10000–24000 cm^{-1} region of the VIS spectrum and a charge transfer band at more than 28000 cm^{-1} (Fig. 6). Two bands centered at ≈18455 cm^{-1} and ≈20880 cm^{-1} appear by increasing the concentration of the studied solution. These have been assigned to the $^4E(^4T_1) \longrightarrow {}^4E(^4T_1(P))$ and $^4E(^4T_1) \longrightarrow {}^4A_2(^4T_1(P))$ transitions respectively, for high-spin Co^{II} ions in a square pyramidal environment.[42b] There is an attempt to form a new band at ≈13000 cm^{-1}, but it is very low and nearly obscured by the baseline.

The VIS spectrum of complex **6** (Fig. 7) shows a broad band in the 10000–18000 cm^{-1} region and a charge transfer band above ≈20000 cm^{-1}. The three absorption bands centered at 13020, 14685 and 16114 cm^{-1} obtained by a Gaussian analysis are in the range typical for five-co-ordinated high-spin Ni^{II}ions with a C_{2v} local symmetry. The corresponding transitions are $^3B_1 \longrightarrow {}^3B_1(^3T_1)$, $^3B_1 \longrightarrow {}^3A_2(^3T_1)$ and $^3B_1 \longrightarrow {}^1A_1(^1D)$, respectively.[42c]

The very broad band at ≈12135 cm^{-1} and the shoulder at ≈10355 cm^{-1} in the visible electronic spectrum of the complex **7** were assigned to the $B_1(d_{x^2-y^2}) \longrightarrow E(d_{xz,yz})$ and $B_1(d_{x^2-y^2}) \longrightarrow B_2(d_{xy})$ transitions, respectively for the Cu^{II} ions in C_{4v} local symmetry.[43]

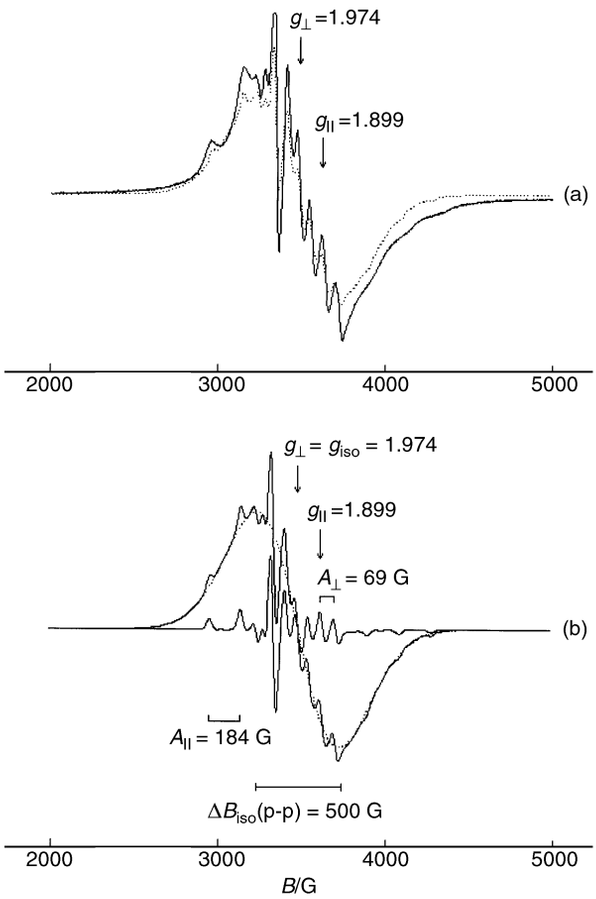

Fig. 8 (a) The experimental powder EPR spectrum of complex **1**, obtained in the X-band at room temperature (normal line) and its simulated spectrum (dotted line). (b) The components of the simulated spectrum of the complex.

EPR and HF-EPR spectroscopy

The powder EPR spectrum of complex **1** based on vanadyl (Fig. 8), obtained in the X-band at room temperature, contains a series of features superposed on a very broad signal. The spectrum was simulated as a superposition of two Gaussian components, an axial and an isotropic one, in a 2 : 3 ratio.

The axial component can be described by the spin Hamiltonian characteristic for one $S = 1/2$ system with C_{4v} symmetry:[44]

$$H = \mu_B[g_{||}B_zS_z + g_\perp(B_xS_x + B_yS_y)] + A_{||}S_zI_z + A_\perp(S_xI_x + S_yI_y) \quad (1)$$

where $g_{||}$, $g_\perp$ and $A_{||}$, $A_\perp$ are the axial principal values of the g and hyperfine tensors respectively, μ_B is the Bohr magneton, B_x, B_y, B_z are the components of the applied magnetic field lengthways of the principal g axes, S_x, S_y, S_z and I_x, I_y, I_z are the components of the electronic and nuclear spin angular momentum operators, respectively. This component exhibits the signals due to the hyperfine coupling of the unpaired electron spin with the nuclear spin of the ^{51}V isotope ($I = 7/2$). ESR parameters of the axial component derived from the simulation are: $g_{||} = 1.899$, $g_\perp = 1.974$, $|A_{||}| = 184$ G, $|A_\perp| = 69$ G and the linewidths $\Delta B_{||}$(p–p) = 57 G, $\Delta B_\perp$(p–p) = 32 G for a Gaussian lineshape. The principal axes of the g and A tensors were presumed to be coincident. Such a low value as that obtained for the parallel component of the g tensor was previously reported for the perpendicular g component of a vanadium disubstituted Keggin type polyoxomolybdate.[45] There, the unpaired electron delocalization responsible for the low g value was due to the proximity of the vanadium and molybdenum ions. In the present case, the vanadium ions are distant enough,[10] the delocalization of the unpaired electron, if present, being achieved only towards the tungsten atoms from the HPOM units, *via* the bonding oxygen atoms. The EPR spectrum contains eight hyperfine lines in each of the parallel and perpendicular bands because of the interaction of one unpaired electron only with a single vanadium nucleus. Therefore, the unpaired electron is predominantly trapped on the parent ion. This behavior helped us to assign the isotropic component, characterized by $g_{iso} = 1.974$ and ΔB_{iso}(p–p) = 500 G. Polyoxometalates with more vanadium ions present such a broad EPR signal with a resolved hyperfine structure due to the electron hopping between the vanadium ions in a thermally activated process[46] or to a clustered system in undiluted powder samples.[47] The intermetallic distance longer than 4.2 Å prevents the electron hopping between the vanadium ions. The broad component of the spectrum could be interpreted in terms of the presence of very weak extended exchange interactions within the vanadyl triangular cluster, as recently reported for the sandwich-type complex with Sb^{III}.[28] These led to the appearance of two doublets ($S = 1/2$) and an excited quartet ($S = 3/2$). This last state could be responsible for the appearance of the broad component of the spectrum, because of the unsolved hyperfine structure and possible g and A tensor's anisotropies.[28]

The degree of covalency of the in-plane V–O π bonds (β_2^2) was evaluated using the LCAO-MO approach for V^{IV} with an antibonding $B_2(d_{xy})$ ground state, in a C_{4v} local symmetry:[40]

$$\beta_2^2 = \frac{7}{6}\left[-\frac{A_{||} - A_\perp}{P} + (g_{||} - g_e) - \frac{5}{14}(g_\perp - g_e)\right] \quad (2)$$

where $P = g_e\mu_B g_N\mu_N\langle r^{-3}\rangle = 0.0128$ cm^{-1} is the dipolar interaction term for the vanadyl ion, $g_e = 2.0023$ is the g factor of the free electron and $\Delta E_{x^2-y^2} = 14705$ cm^{-1} is the energy of the $^2B_2(d_{xy}) \longrightarrow {}^2B_1(d_{x^2-y^2})$ transition obtained from the VIS spectrum. The Fermi contact term was determined as $K = -(A_0/P) - (g_e - g_0)$, where $A_0 = (A_{||} + 2A_\perp)/3$ and $g_0 = (g_{||} + 2g_\perp)/3$. The $\beta_2^2 = 0.876$ value indicates a dominant ionic character of the in-plane π bonds, but there is also a covalent degree to them. The delocalization of the vanadium unpaired electron towards the neighboring oxygen atoms is confirmed by the low $K = 0.705$ Fermi contact term and the negative signs of the $A_{||}$ and $A_\perp$ parameters, the only situation which gives rise to acceptable values for the molecular orbital coefficients.

The EPR parameters and the shape of the spectrum remain nearly unchanged at $T = 80$ K. While the linewidths of the hyperfine signals do not vary when the temperature rises from 80 K to 293 K, the intensity of the whole spectrum strongly decreases. Particularly, the intensity of the $\Delta M_I = -5/2$ hyperfine line decreases by about 23 times. The fact that the proportionality $I \approx 1/T$, where I is the amplitude of the signal, is not observed, points to a non-Curie behavior of the complex due to the V^{IV}–V^{IV} coupling.[48]

HF-EPR spectra of the polycrystalline complex **2**, obtained in W-band (190 GHz) and 5–200 K temperature range (Fig. 9), contain a single broad line at $g \approx 2.0$. By raising the temperature, the linewidth of the signal decreases, which indicates the presence of small Cr^{III}–Cr^{III} superexchange interactions.[2] These can be described by an isotropic exchange Hamiltonian:

$$H_{ex} = -J(S_1S_2 + S_2S_3 + S_1S_3) \quad (3)$$

where J is the isotropic exchange coupling constant between the Cr^{III} ions and S_1, S_2 and S_3 are the electronic spin angular momentum operators of the metallic ions which form an equilateral triangle.

The temperature dependence of the inverse of the linewidth was fitted (Fig. 10) taking into account the proportionality

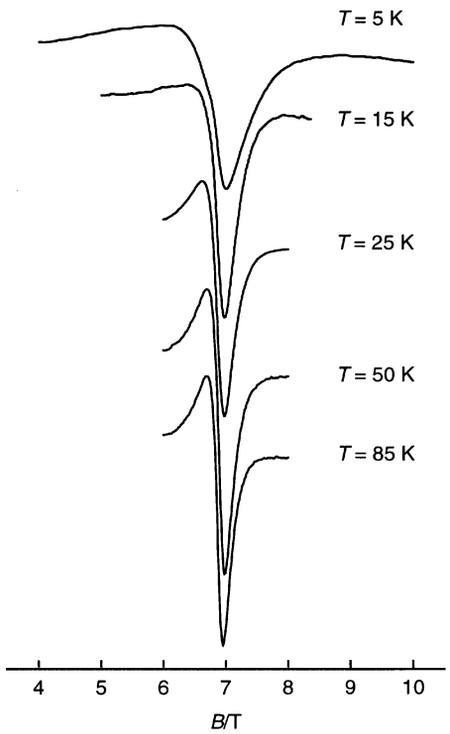

Fig. 9 HF-EPR spectra at 190 GHz of the polycrystalline complex **2** pressed in a pellet, recorded at different temperatures.

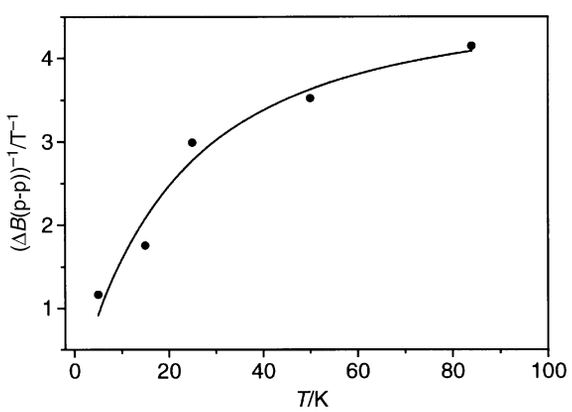

Fig. 10 Temperature dependence of the inverse of the linewidth $(\Delta B(\text{p–p}))^{-1}$ for the HF-EPR signal of the complex **2**. The solid line is the best fit of the data.

$(\Delta B(\text{p–p}))^{-1} \approx \chi_M T$, with χ_M being the molar susceptibility,[49] and in the frame of a HDVV model for three exchange-coupled high-spin Cr^{III} ions ($S_1 = S_2 = S_3 = 3/2$):[50]

$$\chi_M T = (N\mu_B{}^2 g^2/3k)(3x^{3/8} + 60x^{15/8} + 157.5x^{35/8} + 252x^{63/8} + 247.5x^{99/8})/(4x^{3/8} + 16x^{15/8} + 18x^{35/8} + 16x^{63/8} + 10x^{99/8}) \quad (4)$$

where $x = \exp(J/kT)$ and all other parameters have their usual meanings. The best fit was obtained with $J = -4.116$ cm^{-1} taking into account the $g = 1.995$ mean value in the temperature range of 5–85 K. The three Cr^{III} ions are antiferromagnetically coupled as arises from the negative value of the exchange coupling constant. The spin states obtained by coupling antiferromagnetically three $S = 3/2$ spins which form an equilateral triangle are all degenerate except the highest $S = 9/2$ state. The fast relaxation between degenerate states owing to a spin frustration effect makes EPR signals too large and masks the fine structure.

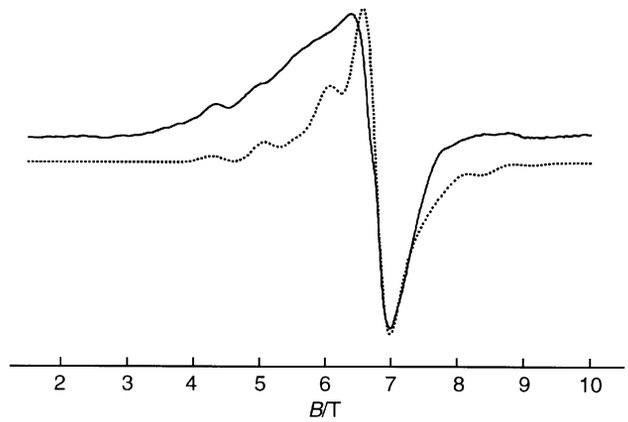

Fig. 11 The HF-EPR spectrum at 190 GHz and $T = 5$ K of a polycrystalline sample of **3** pressed in a pellet. The dotted line represents the simulated spectrum assuming $S = 7/2$.

A large signal ($\Delta B(\text{p–p}) \approx 2800$ G) assigned to coupled Cr^{III} ions is also obtained in the X-band (9.692 GHz) powder spectra, at room and liquid nitrogen temperatures (see ESI). At $T = 80$ K, the signal has increased its intensity by more than 30 times, as compared to the signal at $T = 283$ K. The supplementary signal appearing in the spectrum at $g_2 = 4.047$ is due to $\Delta M_S = \pm 2$ transitions.

EPR spectra of the powder complex **3**, performed in the X-band (9.5 GHz) at room and liquid nitrogen temperatures (see ESI), show an isotropic signal at $g_1 = 2.013$ typical for coupled Mn^{II} ions and a small signal at half-field ($g_2 = 4.264$) due to $\Delta M_S = \pm 2$ transitions. The HF-EPR spectrum of the polycrystalline sample pressed in a pellet, performed in the W-band (190 GHz) at $T = 5$ K exhibits an asymmetric signal at about $g = 2.0$ (Fig. 11), with two well resolved signals in the 4–5 T magnetic field region. Because the complexes containing high-spin Mn^{II} ions usually have g factors near to the $g_e = 2.0023$ free electron value,[49,51] these signals can be attributed to the fine structure of one $S = 7/2$ state. The simulation of the spectrum (Fig. 11) was made with the following EPR parameters: $g = 2.027$, the axial $D = -0.381$ cm^{-1} and rhombic $E = 0.054$ cm^{-1} zero field splitting and the linewidth $\Delta B(\text{p–p}) = 0.35$ T for a Lorentzian lineshape. The asymmetric central part of the spectrum also contains the contribution of the lower spin states obtained by antiferromagnetic coupling between Mn^{II} ions, but there is no evidence of the fine structure arising from these states. Above 15 K, the spectrum changes into a single isotropic signal centered at $g \approx 2.0$ (Fig. 12). The integrated intensity and the linewidth of this signal diminish by increasing the temperature. The exchange coupling constant J was estimated following the same procedure as for the Cr^{III} cluster, but using the $\chi_M T$ expression for three coupled high-spin Mn^{II} ions ($S = 5/2$) forming an equilateral triangle:[10]

$$\chi_M T = (N\mu_B{}^2 g^2/4k)(1 + 20x^{3/2} + 105x^4 + 210x^{15/2} + 330x^{12} + 429x^{35/2} + 455x^{24} + 340x^{63/2})/(1 + 4x^{3/2} + 9x^4 + 10x^{15/2} + 10x^{12} + 9x^{35/2} + 7x^{24} + 4x^{63/2}) \quad (5)$$

with the same significance of x as above.

The best fit (see ESI) was obtained with $J = -2.074$ cm^{-1} taking into account the $g = 2.002$ mean value in the 15–200 K temperature range. The negative coupling constant indicates the presence of antiferromagnetic coupled Mn^{II} ions. The strength of this coupling is smaller than that of the trinuclear Cr^{III} cluster.

The intensity of the signal at $g \approx 2.0$ calculated by integration of the 5.3–8.3 T magnetic field range, decreases on increasing the temperature above 50 K (Fig. 13). The small increase between 25 and 50 K (the plateau of the reciprocal intensity

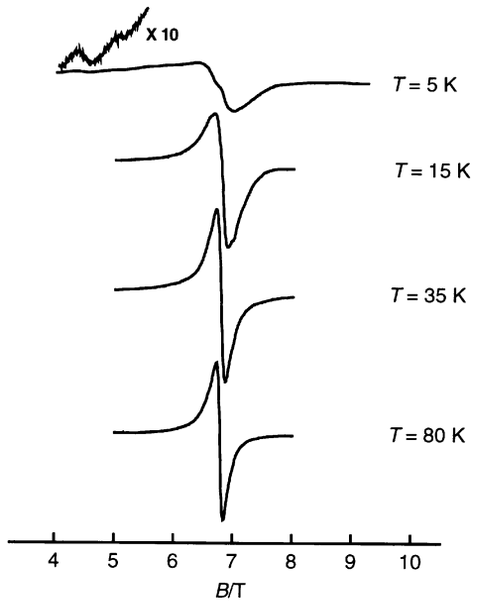

Fig. 12 HF-EPR spectra at 190 GHz of the polycrystalline complex **3** pressed in a pellet, recorded at different temperatures.

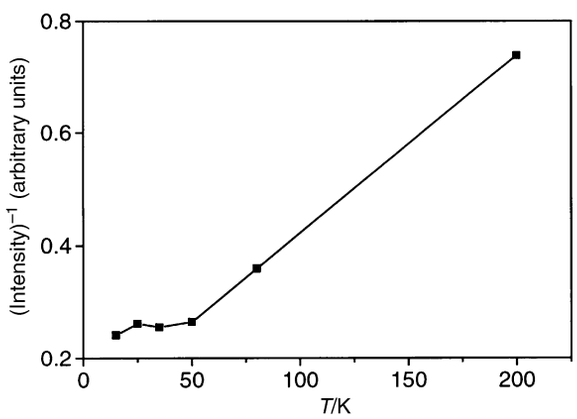

Fig. 13 Temperature dependence of the inverse of the HF-EPR signal intensity for complex **3**.

dependence) is probably due to antiferromagnetic intermolecular interactions.[49]

The powder EPR spectrum obtained in the X-band at $T = 80$ K for complex **4** (Fig. 14a) contains three main features at the effective g values 8.493, 4.289 and 2.000 and a shoulder at 5.498. The g value greater than 6.0 indicates that at this temperature the complex is characterized by one $S \geq 5/2$ spin state.[52] The EPR spectrum was interpreted using an isotropic $S = 5/2$ spin Hamiltonian:[53,54]

$$H = \mu_B BgS + D[S_z^2 - S(S + 1)/3] + E(S_x^2 - S_y^2) \quad (6)$$

The positions of the main signals were reproduced by simulation with an isotropic g tensor, ($g_x = g_y = g_z = 2.0$) and a rhombic fine structure tensor ($D_1 = 1.5$ cm^{-1}, $E_1 = 0.12$ cm^{-1}) (Fig. 14d). However, in the experimental spectrum, the signal at $g_{eff} \approx 4.289$ for transitions in the $M_S = \pm 3/2$ doublet was much more intense than the signal at $g_{eff} \approx 8.493$ for transitions in the $M_S = \pm 1/2$ doublet. This suggested that the experimental spectrum could be rationalized as a superposition of the above component (Fig. 14d) and another component with a stronger signal at $g_{eff} \approx 4.289$.[53] The second component (Fig. 14c), which is present in a 4 : 1 ratio with the first component, also has an isotropic g tensor ($g_x = g_y = g_z = 2.0$) but a greater rhombicity ($D_2 = 1.5$ cm^{-1}, $E_2 = 0.5$ cm^{-1}).

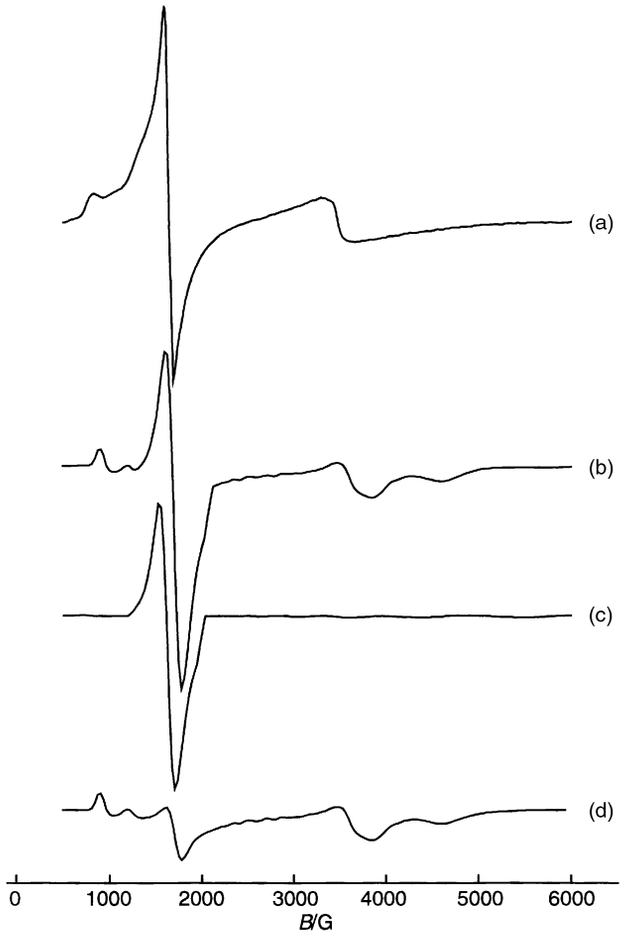

Fig. 14 (a) Powder EPR spectrum of complex **4** obtained in the X-band at 80 K. (b) The total simulated spectrum as a sum of the spectra (c) and (d), assuming $S = 5/2$.

The powder EPR spectrum of complex **5**, recorded in the X-band (9.7 GHz) at $T = 80$ K (see ESI), exhibits a very broad signal (ΔB(p–p) ≈ 2160 G) centered at $g = 3.582$ and a small signal at $g \approx 2.0$. Only the last signal remains in the spectrum when increasing the temperature. The observation of this signal even at room temperature is in good agreement with the presence of coupled Co^{II} ions, with square pyramidal local environments.[55] For the assignment of the signal at $g = 3.582$, we have studied the temperature dependence of the HF-EPR spectra (190 GHz) of the pollycrystaline complex pressed in a pellet (Fig. 15). These spectra exhibit at least four signals. By increasing the temperature from 5 K to 50 K, the feature at lower magnetic fields reveals the presence of two different signals. The ratio of their intensities remains almost constant with changing temperature, which suggests that they originate in the same spin state. The spectrum at 5 K (Fig. 15) is typical for one $S_{eff} = 1/2$ effective state, obtained by antiferromagnetic coupling of the three Co^{II}ions. The cluster has a zero field splitting parameter greater than the millimetric wave energy ($D > 6.3$ cm^{-1}).

The HF-EPR spectrum at $T = 5$ K (Fig. 16) was simulated by superposing in a 2 : 1 ratio the spectra of two distinct species. Each component has $S_{eff} = 1/2$ effective spin and a rhombic g tensor: $g_{x1} = 5.021$, $g_{y1} = 3.561$, $g_{z1} = 2.401$ and $g_{x2} = 5.776$, $g_{y2} = 3.813$, $g_{z2} = 2.850$. The two species could belong to different distorted clusters.

HF-EPR spectra of the polycrystalline sample **6** pressed in a pellet (Fig. 17) contain the most intense signals in the 2–8 T magnetic field region. Their assignment was made after considering the geometry of the cluster of the studied compound and the usual ranges of EPR parameters for the Ni^{II} complexes. The intensity of the signals varies with temperature so that at

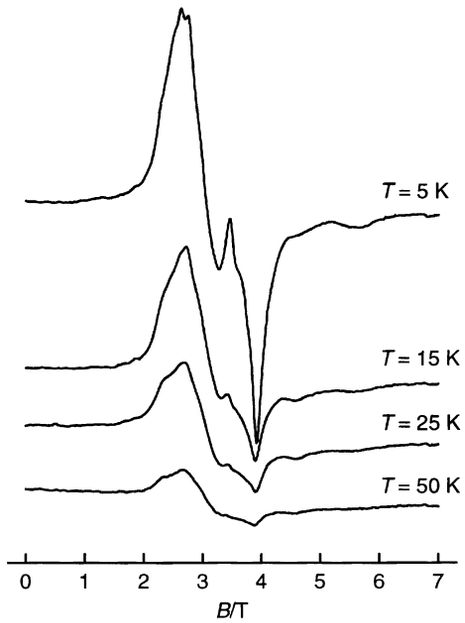

Fig. 15 HF-EPR spectra at 190 GHz of the polycrystalline complex **5** pressed in a pellet, recorded at different temperatures.

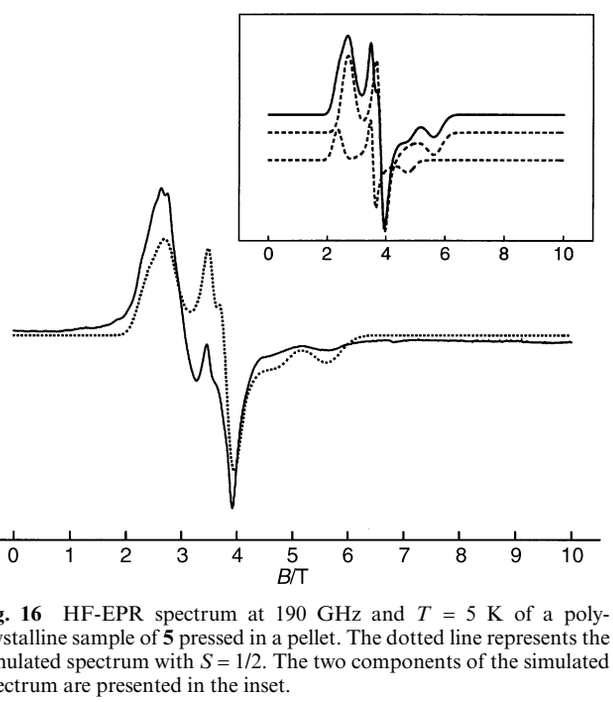

Fig. 16 HF-EPR spectrum at 190 GHz and T = 5 K of a polycrystalline sample of **5** pressed in a pellet. The dotted line represents the simulated spectrum with S = 1/2. The two components of the simulated spectrum are presented in the inset.

25 K three sharp signals and two broader ones are observed. Any attempt to assign the three sharp signals to a fine structure leads to unusually large g values. Taking into account that the extreme signals in the spectra appear at $g \approx 4$ and $g \approx 2$, they were assigned to a $\Delta M_S = \pm 2$ transition and to a double quantum transition, respectively.[56]

The obtained spectra were interpreted in terms of one $S = 1$ spin state for three antiferromagnetic coupled Ni^{II} ions. The main part of the spectrum is due to the $S = 1$ first excited state and the features at lower magnetic fields which are observed at T = 50 K to one excited $S = 2$ state. The $S = 1$ state behavior can be described with a rhombic type Hamiltonian (eqn. (6)). The magnetic fields for $\Delta M_S = \pm 1$ transitions (Fig. 17) estimated from the spectrum at 5 K were used for supplying the EPR parameters by means of a Chasteen procedure.[57] The

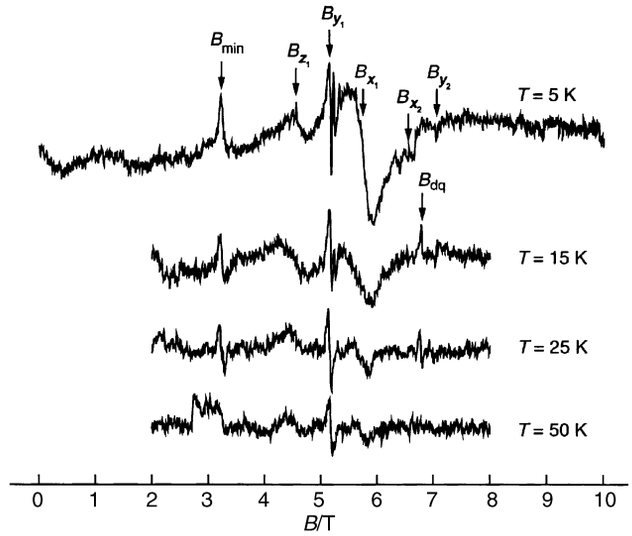

Fig. 17 Temperature dependence of the HF-EPR spectra at 190 GHz of the polycrystalline complex **6** pressed in a pellet.

cluster presents a small rhombic distortion both in g ($g_x = 2.201$, $g_y = 2.211$ and $g_z = 2.292$) and D tensors (D = 1.66 cm^{-1} and $E = 0.18$ cm^{-1}).

The shape of the powder EPR spectrum of complex **7** (see ESI) obtained in the X-band at room temperature is similar to the one which was previously reported for the Cu^{II} trinuclear cluster encapsulated in As^{III} heteropolyanion.[31] The antiferromagnetic coupling between the Cu^{II} ions, favoured by the geometry of the cluster and the spin frustration,[58] leads to a double degenerate S = 1/2 ground state, which is EPR inactive, and one EPR active S = 3/2 excited state. The best fit of the spectrum was obtained with an axial spin Hamiltonian with S = 3/2, principal g values $g_{||} = 2.080$ and $g_{\perp} = 2.237$, the axial zero field splitting parameter D = 0.0214 cm^{-1} and the linewidths $\Delta B_{||} = 106$ G, $\Delta B_{\perp} = 68$ G. The parallel direction is along the C_3 axis of the trinuclear copper cluster and also along the perpendicular direction of the individual g tensors.

Conclusion

Spectroscopic and electron paramagnetic resonance investigations of the sodium/potassium salts of the $[M^{n+}{}_3(H_2O)_x(BiW_9O_{33})_2]^{(18\,-\,3n)-}$ ($M^{n+} = (VO)^{II}$, x = 0 and $M^{n+} = Cr^{III}$, Mn^{II}, Fe^{III}, Co^{II}, Ni^{II}, Cu^{II}, x = 3) heteropolyanions confirms the sandwich-type structure of these complexes and the encapsulation of the trinuclear transition metal cluster between two trivacant Keggin units. FT-IR data indicate the co-ordination of each metallic ion to oxygen atoms from corner-sharing octahedra. The s^2 lone pair on Bi^{III} ions is sterically-inert, at least in the complexes with Cu^{II} and Fe^{III}. The charge transfer into the terminal $W{=}O_t$ bonds is unaffected by the metal ions. The co-ordination of the Cr^{III} and Fe^{III} ions to the trivacant ligand decreases the energy for the charge transfer into the HPOM cage. The LMCT bands (M⟶O) in the VIS spectra are direct proof of the existence of metal–oxygen bonding. Transition metal ions are penta-co-ordinated in square-pyramidal environments and the local symmetry is C_{4v} ($(VO)^{II}$, Cr^{III}, Co^{II}, Cu^{II}) or C_{2v} (Ni^{II}). The ions with more 3d electrons are in a high-spin state.

The three transition metals form a cluster in each sandwich-type complex. In the case of the vanadyl cluster, the unpaired electrons are more trapped on the parent ion and the dipolar V^{IV}–V^{IV} interaction is dominant. The other clusters are based on the superexchange mechanism involving the heteropolyoxometalate unit. The geometry of the triangular cluster and the spin frustration favours the antiferromagnetic interactions.

By means of HF-EPR spectroscopy, the isotropic exchange constants were estimated for the Cr^{III} and Mn^{II} clusters. The *g* tensor is isotropic for Cr^{III}, Mn^{II} and Fe^{III} complexes, axial for $(VO)^{II}$ and Cu^{II} compounds and rhombic for Co^{II} and Ni^{II} complexes. There is a rhombic anisotropy in the zero field splitting tensor of the clusters based on Mn^{II}, Fe^{III} and Ni^{II} ions. Samples of heteropolyoxometalates with Fe^{III} and Co^{II} ions are mixtures of two species, distorted rhombically to different degrees.

Experimental

Measurements

Transition metals, sodium, potassium and bismuth were determined by atomic absorption. The water content was determined on the basis of thermal analysis performed using a METTLER-TGA/SDTA 851ᵉSTARᵉSoftware derivatogaph. FT-IR spectra were recorded on a Jasco FT/IR 610 spectrophotometer in the 4000–200 cm^{-1} range, using KBr pellets. Electronic spectra were performed in aqueous solutions within a range of λ = 190–1000 nm on an ATI Unicam-UV-Visible spectrophotometer with Vision Software V 3.20. EPR spectra on powdered solids were recorded at room temperature and 80 K at *ca.* 9.6 GHz (X-band) using a Bruker ESP 380 spectrometer. W-Band EPR spectra were recorded on the HF-EPR Grenoble spectrometer,[59,60] where the 190 GHz radiation was supplied by a Gunn diode and the absorption of the millimetric waves was detected with a bolometer. Powder samples were pressed in pellets to avoid preferential orientation of the crystallites in the strong magnetic field.

Synthesis

All common laboratory chemicals were reagent grade, purchased from commercial sources and used without further purification. Distilled, deionized water was used throughout.

The synthesis of the sandwich-type heteropolyoxometalate complexes started from a ligand–metallic cation molar ratio of 2 : 3. The $Na_9[BiW_9O_{33}]\cdot 14H_2O$ trivacant ligand was prepared according to the method of Krebs.[61] Complexes were synthesized without controlling the pH. Complex **1** was separated as its potassium salt, with compounds **2**–**7** as sodium salts.

$K_{12}[(VO)_3(BiW_9O_{33})_2]\cdot 31H_2O$ (1). 5.7 g (2 mmol) $Na_9[BiW_9O_{33}]\cdot 14H_2O$ was dissolved in 15 ml of distilled water at 50 °C. Next, 0.54 g (3 mmol) of $VOSO_4\cdot H_2O$ dissolved in 10 ml of distilled water was slowly added at 50 °C while stirring, the mixture stirring subsequently for 15 min. The resulting dark-brown solution was filtered through a medium frit and allowed to cool to room temperature. Finally, ground KCl (1.6 g, 21.5 mmol) was added with stirring to the clear filtrate resulting in the immediate precipitation of a dark-brown product which was recrystallized from a minimum amount of hot water (400 mg/5 ml of water). Dark-brown needle microcrystals of the desired product were obtained within three days. Yield: 3.70 g (62%) (Found: K, 8.00; Bi, 6.89; V, 2.60; W, 54.9; H_2O, 9.09. Calc. for $K_{12}Bi_2W_{18}V_3O_{100}H_{62}$: K, 7.76; Bi, 6.95; V, 2.54; W, 55.08; H_2O, 9.28%).

$Na_9[Cr_3(H_2O)_3(BiW_9O_{33})_2]\cdot 43H_2O$ (2). 5.7 g (2 mmol) $Na_9[BiW_9O_{33}]\cdot 14H_2O$ was dissolved in 15 ml of distilled water (at 50 °C). Next, 0.80 g (3 mmol) of $CrCl_3\cdot 6H_2O$ dissolved in 10 ml of distilled water was slowly added at 50 °C while stirring, the mixture stirring subsequently for 15 min. The resulting dark-green solution was filtered through a medium frit and allowed to cool to room temperature. After four days, a green powder was obtained by filtration and washed with NaCl (2 M), ethanol and diethyl ether. The powder was allowed to crystallize after dissolution in water (200 mg/5 ml). After one week, green parallelepipedic crystals were collected. Yield: 3.29 g (55%) (Found: Na, 3.43; Bi, 6.77; Cr, 2.70; W, 54.97; H_2O, 10.72. Calc. for $Na_9Bi_2W_{18}Cr_3O_{112}H_{92}$: Na, 3.46; Bi, 7.00; Cr, 2.61; W, 55.39; H_2O, 10.86%).

$Na_{12}[Mn_3(H_2O)_3(BiW_9O_{33})_2]\cdot 43H_2O$ (3). 5.7 g (2 mmol) $Na_9[BiW_9O_{33}]\cdot 14H_2O$ was dissolved in 15 ml of distilled water (at 50 °C). Next, 0.74 g (3 mmol) of $Mn(CH_3CO_2)_2\cdot 4H_2O$ dissolved in 10 ml of distilled water was slowly added at 50 °C while stirring, the mixture stirring subsequently for 15 min. The resulting dark-yellow solution was filtered through a medium frit and allowed to cool to room temperature. After eight days, an orange powder was obtained by filtration and washed with NaCl (2 M), ethanol and diethyl ether. The powder was allowed to crystallize after dissolution in water (250 mg/5 ml). After one week, orange needle crystals were collected. Yield: 4.45 g (73%) (Found: Na, 4.35; Bi, 7.00; Mn, 2.58; W, 54.24; H_2O, 13.40. Calc. for $Na_{12}Bi_2W_{18}Mn_3O_{112}H_{93}$: Na, 4.56; Bi, 6.90; Mn, 2.72; W, 54.69; H_2O, 13.65%).

$Na_9[Fe_3(H_2O)_3(BiW_9O_{33})_2]\cdot 37H_2O$ (4). 5.7 g (2 mmol) $Na_9[BiW_9O_{33}]\cdot 14H_2O$ was dissolved in 15 ml of distilled water (at 50 °C). Next, 1.20 g (3 mmol) of $Fe(NO_3)_3\cdot 9H_2O$ dissolved in 10 ml of distilled water was slowly added at 50 °C while stirring, the mixture stirring subsequently for 15 min. The resulting dark-yellow solution was filtered through a medium frit and allowed to cool to room temperature. After one week, a brown-yellow powder was obtained by filtration and washed with NaCl (2 M), ethanol and diethyl ether. The powder was allowed to crystallize after dissolution in water (200 mg/5 ml). After one week brown-yellow parallelepipedic crystals were collected. Yield: 3.20 g (55 %) (Found: Na, 3.38; Bi, 7.24; Fe, 2.68; W, 56.00; H_2O, 12.05. Calc. for $Na_9Bi_2W_{18}Fe_3O_{106}H_{80}$: Na, 3.52; Bi, 7.11; Fe, 2.85; W, 56.30; H_2O, 12.25%).

$Na_{12}[Co_3(H_2O)_3(BiW_9O_{33})_2]\cdot 37H_2O$ (5). 5.7 g (2 mmol) $Na_9[BiW_9O_{33}]\cdot 14H_2O$ was dissolved in 15 ml of distilled water (at 50 °C). Next, 0.87 g (3 mmol) of $Co(NO_3)_2\cdot 6H_2O$ dissolved in 10 ml of distilled water was slowly added at 50 °C while stirring, the mixture stirring subsequently for 15 min. The resulting bluish violet solution was filtered through a medium frit and allowed to cool to room temperature. After two days, a blue powder was obtained by filtration and washed with NaCl (2 M), ethanol and diethyl ether. The powder was allowed to crystallize after dissolution in water (300 mg/5 ml). After three days, red needle crystals were collected. Yield: 4.10 g (69%) (Found: Na, 4.52; Bi, 6.84; Co, 2.82; W, 55.20; H_2O, 11.86. Calc. for $Na_{12}Bi_2W_{18}Co_3O_{106}H_{80}$: Na, 4.63; Bi, 7.02; Co, 2.97; W, 55.56; H_2O, 12.08%).

$Na_{12}[Ni_3(H_2O)_3(BiW_9O_{33})_2]\cdot 39H_2O$ (6). 5.7 g (2 mmol) $Na_9[BiW_9O_{33}]\cdot 14H_2O$ was dissolved in 15 ml of distilled water (at 50 °C). Next, 0.84 g (3 mmol) of $NiSO_4\cdot 7H_2O$ dissolved in 10 ml of distilled water was slowly added at 50 °C while stirring, the mixture stirring subsequently for 15 min. The resulting green-yellow solution was filtered through a medium frit and allowed to cool at room temperature. After three days, a yellow powder was obtained by filtration and washed with NaCl (2 M), ethanol and diethyl ether. The powder was allowed to crystallize after dissolution in water (300 mg/5 ml). After two weeks, yellow parallelepipedic crystals were collected. Yield: 4.28 g (71%) (Found: Na, 4.48; Bi, 6.77; Ni, 2.78; W, 54.95; H_2O, 12.34. Calc. for $Na_{12}Bi_2W_{18}Ni_3O_{108}H_{84}$: Na, 4.60; Bi, 6.98; Ni, 2.90; W, 55.27; H_2O,12.62%).

$Na_{12}[Cu_3(H_2O)_3(BiW_9O_{33})_2]\cdot 29H_2O$ (7). 5.7 g (2 mmol) $Na_9[BiW_9O_{33}]\cdot 14H_2O$ was dissolved in 15 ml of distilled water (at 50 °C). Next, 0.60 g (3 mmol) of $Cu(CH_3CO_2)\cdot H_2O$ dissolved in 10 ml of distilled water was slowly added at 50 °C while stirring, the mixture stirring subsequently for 15 min. The

resulting yellow-green solution was filtered through a medium frit and allowed to cool to room temperature. After four days, a yellow-green powder was obtained by filtration and washed with NaCl (2 M), ethanol and diethyl ether. The powder was allowed to crystallize after dissolution in water (400 mg/5 ml). After three days, yellow prismatic crystals were collected. Yield: 4.33 g (74%) (Found: Na, 4.82; Bi, 7.16; Cu, 3.28; W, 56.70; H_2O, 9.89. Calc. for $Na_{12}Bi_2W_{18}Cu_3O_{98}H_{64}$: Na, 4.74; Bi, 7.14; Cu, 3.30; W, 56.81; H_2O, 9.82%).

Thermogravimetric studies

Thermogravimetric studies were carried out on a 20 mg sample of complex at a heating rate of 10 °C min^{-1}. The TG curves exhibited two distinct steps. The first step, below 130 °C, corresponds to the loss of lattice water (endothermic) and the second step, in the 260–305 °C range, corresponds to the loss of three water molecules per metal atom (endothermic) from complexes **2**–**7**. The loss of water at such a high temperature indicates that these water molecules are co-ordinated. Above 400 °C, the inorganic residue exhibits some minor exothermal effect, probably due to a polymorphic transformation of the metal oxide mixture.

Acknowledgements

This work was supported by the Grants B10-6235 and B05-6203 from the National Agency of Science, Technology and Invention, which is gratefully acknowledged. C.C. and L.D. are deeply grateful for the support of the European Community "Access to Research Infrastructure action of the Improving Human Potential Programme" which facilitated the HF-EPR measurements (SO-1201).

References

1 E. Coronado and C. J. Gómez-Garciá, *Chem. Rev.*, 1998, **98**, 273.
2 A. Müller, F. Peters, M. T. Pope and D. Gatteschi, *Chem. Rev.*, 1998, **98**, 239.
3 H. Andres, J. M. Clemente-Juan, R. Basler, M. Aebersold, H.-V. Güdel, J. J. Borrás-Almenar, A. Gaita, E. Coronado, H. Büttuer and S. Janssen, *Inorg. Chem.*, 2001, **40**, 1943.
4 Y. Inouye, Y. Fujimoto, M. Sugiyama, T. Yoshida and T. Yamase, *Biol. Pharm. Bull.*, 1995, **18**, 996.
5 D. L. Barnard, C. L. Hill, T. Gage, J. E. Matheson, J. H. Huffman, R. W. Sidwell, M. I. Otto and R. F. Schinazi, *Antiviral Res.*, 1997, **34**, 27.
6 X. Zhang, Q. Chen, D. C. Duncan, C. F. Campana and C. L. Hill, *Inorg. Chem.*, 1997, **36**, 4208.
7 R. Neumann and A. M. Khenkin, *Inorg. Chem.*, 1995, **34**, 5753.
8 X. Zhang, T. M. Anderson, Q. Chen and C. L. Hill, *Inorg. Chem.*, 2001, **40**, 418.
9 J. M. Clemente-Juan, E. Coronado, J. R. Galán-Mascarós and C. J. Gómez-Garciá, *Inorg. Chem.*, 1999, **38**, 55.
10 P. Mialane, J. Marrot, E. Rivière, J. Nebout and G. Hervé, *Inorg. Chem.*, 2001, **40**, 44.
11 N. Casãn-Pastor, J. Bas-Serra, E. Coronado, G. Pourroy and L. C. W. Baker, *J. Am. Chem. Soc.*, 1992, **114**, 10380.
12 H. T. Evans, C. M. Tourné, G. F. Tourné and T. J. R. Weakley, *J. Chem. Soc., Dalton Trans.*, 1986, 2699.
13 L.-H. Bi, R.-D. Huang, J. Peng, E.-B. Wang, Y.-H. Wang and C.-W. Hu, *J. Chem. Soc., Dalton Trans.*, 2001, 121.
14 D. Gatteschi, *Adv. Mater.*, 1994, **6**, 635.
15 Y. P. Jeannin, *Chem. Rev.*, 1998, **98**, 51.
16 I. Loose, E. Droste, M. Bössing, H. Pohlmann, M. H. Dickman, C. Rosu, M. T. Pope and B. Krebs, *Inorg. Chem.*, 1999, **38**, 2688.
17 Y. P. Jeannin and J. Martin-Frère, *J. Am. Chem. Soc.*, 1981, **103**, 1664.
18 T. J. R. Weakley, *Inorg. Chim. Acta*, 1984, **87**, 13.
19 A. Müller, E. Krickemeyer, S. Dillinger, J. Meyer, H. Bögge and A. Stammler, *Angew. Chem.*, 1996, **108**, 183.
20 J. Fischer, L. Ricard and R. Weiss, *J. Am. Chem. Soc.*, 1976, **98**, 3050.
21 T. Yamase, H. Naruke and Y. Sasaki, *J. Chem. Soc., Dalton Trans.*, 1990, 1687.
22 M. Bössing, A. Noh, I. Loose and B. Krebs, *J. Am. Chem. Soc.*, 1998, **120**, 7252.
23 C. Rosu, M. Rusu, N. Casãn-Pastor and C. J. Gómez-Garciá, *Synth. React. Inorg. Met.-Org. Chem.*, 2000, **30**, 369.
24 M. Bosing, A. Noh, I. Loose and B. Krebs, *J. Am. Chem. Soc.*, 1998, **120**, 7252.
25 B. Krebs, E. Droste, M. Piepenbrink and G. Vollmer, *C. R. Acad. Sci. Paris Serie IIIc*, 2000, **3**, 205.
26 Y. Ozava and Y. Sasaki, *Chem. Lett.*, 1987, 923.
27 B. Botar, T. Yamase and E. Ishikawa, *Inorg. Chem. Commun.*, 2000, **3**, 579.
28 T. Yamase, B. Botar, E. Ishikawa and K. Fukaya, *Chem. Lett.*, 2001, **1**, 56.
29 F. Robert, M. Leyrie and G. Hervé, *Acta Crystallogr., Sect. B*, 1982, **38**, 358.
30 M. T. Pope, in *Heteropoly and Isopoly Oxometalates*, Springer-Verlag, Berlin, 1983, p. 88.
31 Y. H. Cho and H. So, *Bull. Korean Chem. Soc.*, 1995, **16**, 243.
32 C. Rocchiccioli-Deltcheff and R. Thouvenot, *C. R. Seances Acad. Sci., Ser. C*, 1974, **278**, 857.
33 C. J. Gómez-Garciá, C. Giménez-Saiz, S. Triki, E. Coronado, P. Le Magueres, L. Ouahab, L. Ducasse, C. Sourisseau and P. Delhaes, *Inorg. Chem.*, 1995, **34**, 4139.
34 R. Contant, M. Abbesi and J. Canny, *Inorg. Chem.*, 1997, **36**, 961.
35 W. H. Knoth, P. J. Domaille and R. L. Harlow, *Inorg. Chem.*, 1986, **25**, 1577.
36 R. Massart, R. Contant, J. M. Fruchart, J. F. Ciabrini and M. Fournier, *Inorg. Chem.*, 1977, **16**, 2916.
37 T. Yamase, *Chem. Rev.*, 1998, **98**, 307.
38 H. So and M. T. Pope, *Inorg. Chem.*, 1972, **11**, 1441.
39 E. Cadot, M. Fournier, A. Tézé and G. Hervé, *Inorg. Chem.*, 1996, **35**, 282.
40 A. Bencini and D. Gatteschi, in *Transition Metal Chemistry*, Marcel Dekker, New York, 1982, vol. 8, p. 59.
41 J. R. Campbell and R. J. H. Clark, *Chem. Commun.*, 1980, 772.
42 (*a*) A. B. P. Lever, in *Inorganic Electronic Spectroscopy*, Elsevier, New York, 2nd edn., 1984, p. 450; (*b*) A. B. P. Lever, in *Inorganic Electronic Spectroscopy*, Elsevier, New York, 2nd edn., 1984, p. 487; (*c*) A. B. P. Lever, in *Inorganic Electronic Spectroscopy*, Elsevier, New York, 2nd edn., 1984, p. 520.
43 B. J. Hathaway, in *Comprehensive Coordination Chemistry*, ed. G. Wilkinson, Pergamon Press, Oxford, 1987, vol. 5, p. 678.
44 J. Park and H. So, *Bull. Korean Chem. Soc.*, 1994, **15**, 752.
45 M. Otake, Y. Komiyama and T. Otaki, *J. Phys. Chem.*, 1973, **77**, 2896.
46 C. W. Lee and H. So, *Bull. Korean Chem. Soc.*, 1986, **7**, 318.
47 A. Bencini and D. Gatteschi, in *EPR of Exchange Coupled Systems* Springer-Verlag, Berlin, 1990, p. 137.
48 D. Collison, D. R. Eardley, F. E. Mabbs, A. K. Powell and S. S. Turner, *Inorg. Chem.*, 1993, **32**, 664.
49 V. Tangoulis, D. A. Malamatari, K. Soulti, V. Stergiou, C. P. Raptopoulou, A. Terzis, T. A. Kabanos and D. P. Kessissoglou, *Inorg. Chem.*, 1996, **35**, 4974.
50 O. Kahn, in *Molecular Magnetism*, VCH Publishers, Inc., New York, 1993, p. 212.
51 D. M. L. Goodgame, M. Goodgame and P. J. Hayward, *J. Chem. Soc., A*, 1970, 1352.
52 J. Moura, A. Macedo and J. J. G. Moura, in *Advanced EPR. Applications in Biology and Biochemistry*, ed. A. J. Hoff, Elsevier, Amsterdam, 1989, p. 816.
53 C. R. Staples, I. K. Dhawan, M. G. Finnegan, D. A. Dwinell, Z. H. Zhou, H. Huang, M. F. J. M. Verhagen, M. W. W. Adams and M. K. Johnson, *Inorg. Chem.*, 1997, **36**, 5740.
54 J. J. Girerd, G. C. Papaefthymiou, A. D. Watson, E. Gamp, K. S. Hagen, N. Edelstein, R. B. Frankel and R. H. Holm, *J. Am. Chem. Soc.*, 1984, **106**, 5941.
55 R. S. Drago, in *Physical Methods for Chemists*, Saunders, Philadelphia, 2nd edn., 1977, p. 587.
56 L. A. Pardi, A. K. Hassan, F. B. Hulsbergen, J. Reedijk, A. L. Spek and L.-C. Brunel, *Inorg. Chem.*, 2000, **39**, 159.
57 N. D. Chasteen, *Inorg. Chem.*, 1971, **10**, 2339.
58 P. Chaudhuri, M. Winter, B. P. C. D. Vedova, E. Bill, A. Trautwein, S. Gehring, P. Fleischhaner, B. Nuber and J. Weiss, *Inorg. Chem.*, 1991, **30**, 2148.
59 F. Muller, M. A. Hopkins, N. Coron, M. Grynberg, L. C. Brunel and G. Martinez, *Rev. Sci. Instrum.*, 1989, **60**, 3681.
60 A. L. Barra, L. C. Brunel and J. B. Robert, *Chem. Phys. Lett.*, 1990, **165**, 107.
61 B. Krebs and R. Klein, in *Polyoxometalates: From Platonic Solids to Anti-Retroviral Activity*, ed. M. T. Pope and A. Müller, Kluwer Publishers, Dordrecht, 1994, p. 47.